



HAL
open science

Simulation of West African monsoon circulation in four atmospheric general circulation models forced by prescribed sea surface temperature

Vincent Moron

► **To cite this version:**

Vincent Moron. Simulation of West African monsoon circulation in four atmospheric general circulation models forced by prescribed sea surface temperature. *Journal of Geophysical Research*, 2004, 109 (D24), 10.1029/2004JD004760 . hal-02895236

HAL Id: hal-02895236

<https://hal.science/hal-02895236>

Submitted on 1 Feb 2021

HAL is a multi-disciplinary open access archive for the deposit and dissemination of scientific research documents, whether they are published or not. The documents may come from teaching and research institutions in France or abroad, or from public or private research centers.

L'archive ouverte pluridisciplinaire **HAL**, est destinée au dépôt et à la diffusion de documents scientifiques de niveau recherche, publiés ou non, émanant des établissements d'enseignement et de recherche français ou étrangers, des laboratoires publics ou privés.

Simulation of West African monsoon circulation in four atmospheric general circulation models forced by prescribed sea surface temperature

Vincent Moron,^{1,2,3} Nathalie Philippon,^{4,5} and Bernard Fontaine⁴

Received 11 March 2004; revised 3 September 2004; accepted 18 October 2004; published 23 December 2004.

[1] The mean evolution of the West African monsoon (WAM) circulation and its interannual variability have been studied using an ensemble of 21 simulations (common period 1961–1994) performed with four different atmospheric general circulation models (AGCMs) (European Center/Hamburg (ECHAM) 3, ECHAM 4, Action de Recherche Petite Echelle Grande Echelle (ARPEGE), and Goddard Institute for Space Studies (GISS)) and forced by the same observed sea surface temperature (SST) data set. The results have been compared with European Centre for Medium-Range Weather Forecasts reanalyses (ERA-40). The climatological means of WAM winds for the AGCMs are similar to the ERA-40 ones. However, the AGCMs tend to underestimate the southern wind component at low levels around 10°N compared to the ERA-40. The simulated Tropical Easterly Jet (TEJ) is usually shifted northward and also too weak for ECHAM 3 and ECHAM 4 compared to ERA-40. The interannual variability of an atmospheric WAM index (WAMI) is quite successfully reproduced (the correlations between the mean ensemble of each AGCM and ERA-40 time series over 1961–1994 range between 0.51 and 0.64). In particular, the four AGCMs reproduce quite well the mean teleconnection structure with El Niño–Southern Oscillation, i.e., a strong (weak) monsoon during La Niña (El Niño) events, even if the largest absolute correlations between WAMI and SST in the eastern and central equatorial Pacific are weaker than in ERA-40. On a yearly basis, WAMI is more predictable and skillful during the cold ENSO years than during the warm ENSO ones. The unskillful warm ENSO events are associated with a significant cooling over the equatorial Atlantic and Western Pacific Ocean and a significant warming in the tropical Indian Ocean. *INDEX TERMS:* 1620 Global Change: Climate dynamics (3309); 1610 Global Change: Atmosphere (0315, 0325); 3309 Meteorology and Atmospheric Dynamics: Climatology (1620); 3337 Meteorology and Atmospheric Dynamics: Numerical modeling and data assimilation; *KEYWORDS:* West African summer monsoon circulation, atmospheric general circulation model, sea surface temperature, skill, reproducibility

Citation: Moron, V., N. Philippon, and B. Fontaine (2004), Simulation of West African monsoon circulation in four atmospheric general circulation models forced by prescribed sea surface temperature, *J. Geophys. Res.*, 109, D24105, doi:10.1029/2004JD004760.

1. Introduction

[2] The West African monsoon (WAM) is a recurrent large-scale pattern arising from the thermal contrast existing between the warm African continent and the adjacent cooler southern Atlantic Ocean. Interannual and interdecadal vari-

ability of WAM have been subject to many observational and numerical studies, mainly through the relationships between seasonal Sahelian rainfall variability and large-scale sea surface temperature (SST) patterns [e.g., Folland *et al.*, 1986, 1991; Druyan, 1989; Hastenrath, 1990; Ward, 1992, 1998; Fontaine and Bigot, 1993; Rowell *et al.*, 1995; Trzaska *et al.*, 1996; Fontaine and Janicot, 1996; Rowell, 2001]. Comparatively, only a few studies have investigated the physical relationship between WAM dynamics, identified through Tropical Easterly Jet (TEJ) and/or monsoon flow anomalies, and large-scale SST variability [Palmer *et al.*, 1992; Fontaine *et al.*, 1995; Moron *et al.*, 1995; Janicot *et al.*, 1998, 2001]. All these studies indicate strong links between weakened TEJ [Palmer *et al.*, 1992; Janicot *et al.*, 2001], enhanced trade winds over the north tropical Atlantic and weaker moisture advection over West Africa, consistent with weaker monsoon and Southern Hemisphere Hadley circulation during warm El Niño Southern Oscillation

¹UFR des Sciences Géographiques et de l'Aménagement, Université d'Aix-Marseille I, Aix en Provence, France.

²Centre Européen de Recherche et d'Enseignement des Géosciences de l'Environnement, UMR 6635, CNRS, Aix en Provence, France.

³Also at International Research Institute for Climate Prediction, Palisades, New York, USA.

⁴Centre de Recherches de Climatologie, UMR 5080, CNRS, Dijon, France.

⁵Centre d'Études Spatiales de la Biosphère, Centre National d'Études Spatiales, CNRS, Toulouse, France.

(ENSO) events [Janicot *et al.*, 1998, 2001; Rowell, 2001]. WAM dynamics at the regional scale are also a response to the north-south thermal gradient across the tropical Atlantic at the source of the migration of the Intertropical Convergence Zone [Hastenrath, 1990; Fontaine and Janicot, 1996].

[3] The El Niño seasonal predictability [e.g., Palmer and Anderson, 1994; Goddard *et al.*, 2001] as well as sea surface thermal inertia make WAM potentially predictable from SST anomalies (SSTA hereafter). This potential predictability provided by SST forcing can be partly estimated using ensembles of atmospheric GCMs integrations forced by prescribed SST [Gates, 1992; Sperber and Palmer, 1996]. In the tropics, a strong reproducibility (i.e., the AGCM's variance that is independent from initial conditions), and thus a strong potential predictability from SSTA, is usually associated with a high skill (i.e., the ability to simulate the observed anomaly) [Moron *et al.*, 1998]. The statistical estimates of reproducibility and/or skill found in previous studies are almost always given through seasonal Sahelian rainfall estimates. However, AGCMs show poor reproducibility and skill especially when the decadal-scale trend is removed [Rowell *et al.*, 1995; Srinivasan *et al.*, 1995; Sperber and Palmer, 1996; Moron *et al.*, 2003].

[4] The main objectives of this study are therefore to evaluate (1) the AGCM ability to simulate the monsoonal circulation over West Africa in terms of both intensity and seasonal evolution and to correctly respond to the imposed surface forcing, in particular the one associated with the ENSO phenomenon; (2) the intensity and significance of the interannual SST forcing and (3) the skill of AGCMs. We concentrate here on several large-scale wind indices, involving the lower and upper levels of the WAM, rather than the regional rainfall index, because (1) AGCMs perform better in capturing the large-scale dynamic fluctuations than the regional-scale rainfall variations [Sperber and Palmer, 1996; Garric *et al.*, 2002; Cherchi and Navarra, 2003] and (2) such wind indices are strongly related to the observed regional-scale rainfall variations, giving then the advisability of an efficient statistico-dynamical prediction of rainfall [Garric *et al.*, 2002]; for example, the correlation between the main wind index used in this study (i.e., West African Monsoon Index (WAMI) defined in terms of the shear between the wind speed at the summit of the monsoon flow and the Tropical Easterly Jet) from ERA-40 and an observed regional Sahelian rainfall index (SRI) such as the one defined by Moron *et al.* [2003] over 1961–1994 is 0.78. Thus it appears important to establish the reproducibility and skill of these large-scale wind indices. Twenty-one runs from four AGCMs (European Center/Hamburg (ECHAM) 3 and 4, Action de Recherche Petite Echelle Grande Echelle (ARPEGE), and Goddard Institute for Space Studies (GISS) 2000) are used in an ensemble approach to evaluate the ability of these AGCMs to reproduce the seasonal and interannual variability of the WAM wind indices. The members of the ensemble have the same boundary conditions (SST from Global Ice and Sea Surface Temperature data set [Rayner *et al.*, 1996]) but differences in initial conditions, horizontal and vertical resolutions and parameterizations. Using four AGCMs forced by the same boundary forcing is a way of taking into account our uncertainty about the representation of the atmospheric laws. Moreover, previous studies [e.g., Srinivasan *et al.*, 1995; Sperber and

Palmer, 1996; Sud and Lau, 1996; Gadgil and Sajani, 1998] indicate a large spread in simulations of the WAM variability, and a strong model dependence, especially for the first AMIP I time period (1979–1988). The intensity of SST forcing and skill is evaluated using traditional scores (such as linear correlation) but also probabilistic scores considering the probability density function (PDF) of the 21 runs rather than their ensemble mean. This approach allows a better representation of the possible outcomes associated with a particular SST forcing.

[5] The study is divided into six sections. Section 2 details the selected simulations, reanalyses and methods used. Section 3 presents the climatology of the West African monsoon as simulated by each AGCM with comparisons mainly with ERA-40 reanalyses. Section 4 analyzes the interannual variability of the monsoon and its teleconnection patterns with SST in ERA-40 and each AGCM. Attention is focused on extreme ENSO years, since ENSO is known to provide a major forcing on WAM [Palmer *et al.*, 1992; Janicot *et al.*, 1996, 2001; Rowell, 2001]. Section 5 concerns the yearly analysis of reproducibility and skill. An overall summary is provided in section 6.

2. Data and Methods

2.1. AGCM Runs

[6] The AGCMs used in this study have been presented elsewhere (Deutsches Klimarechenzentrum (DKRZ) [1993] for ECHAM, Déqué *et al.* [1994] for ARPEGE, and Hansen *et al.* [2002] for GISS). Only a short description is given here [see also Moron *et al.*, 2003].

[7] ECHAM 3 and ECHAM 4 are the third and fourth generations of a climate model originating from the ECMWF spectral medium range weather forecast model developed at the Max Planck Institute in Hamburg. Details of ECHAM 3 numerical formulation and physical parameterizations are given by DKRZ [1993]. ARPEGE is the third version of the ARPEGE-Climat model developed at Météo-France from the ARPEGE/IFS operational weather prediction model [Déqué *et al.*, 1994]. ECHAM 3, ECHAM 4 and ARPEGE are spectral models with a T21 (~5.6 by 5.6 degree grid), T30 (~3.75 by 3.75 degree grid) and T63 (~1.9 by 1.9 degree grid) horizontal resolution, respectively. Note that the ARPEGE runs used here are available on a T42 (~2.8 by 2.8 degree grid) horizontal resolution. The vertical is divided into 31 levels in ARPEGE and 19 levels in ECHAM 3 and ECHAM 4. For these three models, the 850 hPa and 200 hPa levels are used to represent the lower and upper levels of the monsoonal circulation, respectively. GISS-2000 (GISS hereafter) is developed at the Goddard Institute for Space Studies. It is a grid point model with 72 points in longitude and 46 points in latitude, giving a 5 by 4 degree grid; there are 12 levels in the vertical [Hansen *et al.*, 2002]. For GISS, the 850 hPa and 200 hPa levels are not available and are replaced by the closest levels, i.e., 894 and 247 hPa.

[8] These four AGCMs use basic atmospheric physical parameterizations as well as comprehensive land surface schemes (LSS) that describe explicitly some vegetation processes such as interception and re-evaporation of rain and extraction of soil moisture. ECHAM 3 and ECHAM 4 use a modified “bucket” LSS [DKRZ, 1993], even though

GISS and ARPEGE use more sophisticated LSS [Douville and Chauvin, 2000; Douville et al., 2001; Douville, 2002].

[9] The runs analyzed have also already been presented (e.g., Moron et al. [1998, 2001] for ECHAM 3 and ECHAM 4; Cherchi and Navarra [2003] for ECHAM 4; Cassou and Terray [2001] for ARPEGE; and Hansen et al. [2002] for GISS) and were performed with Global Ice Sea Surface Temperature (GISST) version 2 [Rayner et al., 1996]. All other external atmospheric forcings (solar radiation input, CO₂ concentration, etc.) are kept at their standard values. A total of 21 runs are analyzed: 8 for ARPEGE, 5 for ECHAM 3 and GISS, and 3 for ECHAM 4; they only differ by their initial conditions.

2.2. Reanalyses

[10] The second generation of reanalyses provided by the European Centre for Medium-Range Weather Forecasts (ERA-40; <http://www.ecmwf.int/research/era>) covers the period from September 1957 and has the benefit of knowing many of the problems encountered in the first generation of reanalyses provided by the National Center for Environmental Prediction (NCEP I) [Kalnay et al., 1996]. The horizontal resolution of the Integrated Forecasting System spectral model used for ERA-40 is T159, and there are 60 levels in the vertical. Historical ground-based observations as well as information from satellite (from 1972) are used in the three-dimensional assimilation scheme [Uppala, 2002]. The data are available on a 2.5 by 2.5 degree grid at <http://www.ecmwf.int/research/demeter> and could be considered as the best available surrogate to actual observations. We must also keep in mind that ERA-40 (and NCEP I, see below) are, in fact, not observations and remain just one integration of a sophisticated GCM.

[11] The first generation of reanalyses provided by the NCEP (NCEP I) [Kalnay et al., 1996] is now available from 1949 (for example, from <http://ingrid.ldgo.columbia.edu/SOURCES/NCEP-NCAR/>). The horizontal resolution of the NCEP model is T62 (with a resulting 2.5 × 2.5 degree grid), and there are 28 levels in the vertical. The main problems in NCEP I, and particularly relevant over the West African window, concern the period 1958–1967 when few “in situ” data enter the model, as well as the end of the 1970s when remote-sensing data start being assimilated; this creates severe shifts in time series (see Figure 5) [Poccard et al., 2000; Camberlin et al., 2001; Janicot et al., 2001].

2.3. Methods

[12] The analysis of a range of AGCM runs forced by the same SST forcing relies on the fact that boundary forcing, as SST, could alter the phase-space geometry of the whole atmospheric attractor [Palmer, 1993; Kumar and Hoerling, 1995]. A single realization of an AGCM experiment (equals a “run”) with observed temporally varying SST contains not only the effect of the underlying SST but also chaotic variations associated with nonlinear atmospheric dynamics. Considering a range of runs with different initial conditions allows the separation of the “SST-forced” (or external) variance [Rowell et al., 1995; Kumar and Hoerling, 1995; Rowell, 1998], potentially predictable from SST if these last are known in advance, and internal unpredictable variance (or “noise”). However, different AGCMs could respond to the same SST forcing in different ways; so a multi-AGCM

ensemble (with multiple runs for each AGCM) allows one to consider AGCMs differences also. The SST impact can be measured in terms of changes in the PDF of the atmospheric state, here defined through large-scale wind indices related to WAM circulation. In the tropics, it is well known that the effect of interannual SST variations is to create a detectable shift in the atmosphere’s mean state [Kumar and Hoerling, 1995; Stern and Miyakoda, 1995], but this effect could also be a reduction of the spread of the possible outcomes without any significant shift of the mean [Anderson and Stern, 1996]. Various scores have been used to measure the deterministic and probabilistic information provided by an ensemble of AGCMs runs. The ensemble mean gives, on average, a better skill than an individual forecast, but it does not provide all the information contained in the ensemble. Two probabilistic scores (Kuiper statistic (KS) and rank probability skill score (RPSS)) have been also used here to take advantage of the full ensemble information.

[13] The reproducibility of WAMI is estimated with KS [Anderson and Stern, 1996; Jetsu and Pelt, 1996]. The null hypothesis is that two independent samples have been drawn from the same continuous probability distribution. In this study, the first sample is made of the 21 runs of a given year i whereas the second sample is constituted of the 21 runs of the $n - i$ remaining years (i.e., 21 × 33 runs), which gives a rough estimate of the “climatological” PDF [Anderson and Stern, 1996]. KS ranges theoretically between 0 and 1; large values suggest that the two samples can be assumed to come from different continuous distributions [Jetsu and Pelt, 1996], so that SST provides a significant forcing.

[14] The predictability estimated with KS is only potential since the performance of a model in simulating observed WAMI (called the skill of the model hereafter) could also be weakened by (1) systematic errors in AGCMs and (2) intervention of forcing factors other than SST. AGCM skill for each year is here evaluated through the rank probability skill score (RPSS) [Doblas-Reyes et al., 2000]. The rank probability score [Epstein, 1969] measures the overall forecast performance of the ensemble of 21 runs. The 34 observations (after having standardized WAMI to zero mean and unit variance) are first distributed into three almost equiprobable categories (with 12, 10 and 12 members, respectively). Each run is standardized over the 1961–1994 period. The 21 runs of a given year are then distributed into these three categories, and the corresponding forecast cumulative distribution is obtained. The observation occurs, of course, in only one category. RPS for one forecast is the sum of the squared errors of the cumulative distributions. A perfect forecast would assign all of the probability to the same category in which the observation occurs, resulting in an RPS of 0. The RPSS expresses the relative improvement of the forecast against a reference forecast (here, the climatology) and is 100% for a perfect forecast, 0% for a trivial forecast and even negative values when the forecast concentrates its probability far from the observed category [Doblas-Reyes et al., 2000].

3. Climatology

[15] The climatology of the upper and lower levels of the WAM in August is displayed for ERA-40 (Figure 1) and

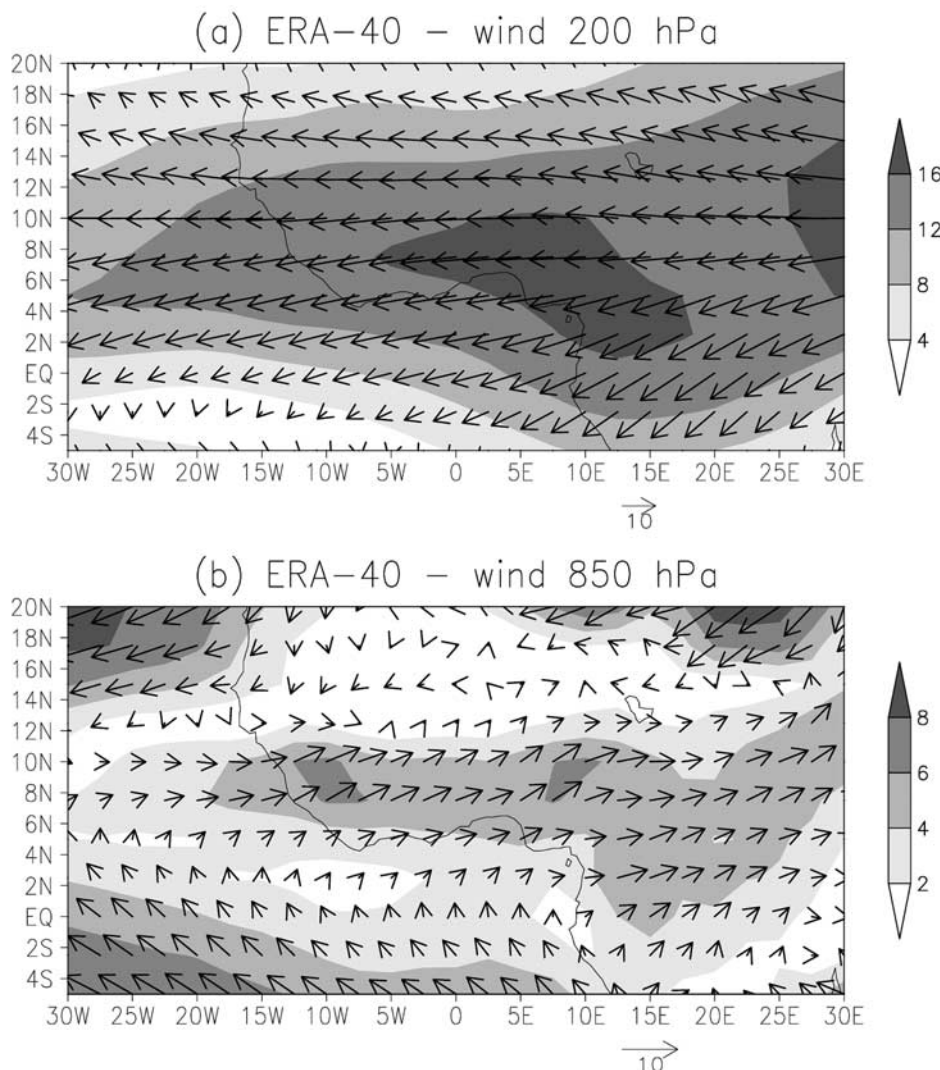


Figure 1. Mean wind (arrows) and modulus of the wind (shading) in m/s in August at (a) 200 hPa and (b) 850 hPa from ERA-40 (period 1958–2001). The vector scale is indicated at the bottom of each panel.

each AGCM (200 hPa (Figure 2) and 850 hPa (Figure 3)). In northern summer, strong easterlies in the upper troposphere and strong southwesterlies in the lower troposphere prevail over the entire West African monsoon area, as shown in Figure 1 for the month of August. At low levels (Figure 1b) the southwest monsoon flow registers maxima near 7.5°N whereas in the upper troposphere the mean flow is dominated by the Tropical Easterly Jet (TEJ), which peaks (around 17 m/s) above southern Nigeria and exhibits weak divergence across its main axis (Figure 1a). If the mean TEJ latitudinal position and intensity are successfully simulated by ARPEGE (Figure 2a), they appear too weak and too northerly in the ECHAM 4 (Figure 2b) and ECHAM 3 (Figure 2c) simulations. This is in agreement with previous studies. *Cherchi and Navarra* [2003], analyzing the same ensemble of ECHAM 4, also found that TEJ is weaker than in the ERA-15 reanalyses over the Indian Ocean. TEJ is also weaker in GISS than in ERA-40 (Figure 2d) but is not shifted northward. The northward component of the low-level monsoon flow is usually weaker in AGCMs than in ERA-40 (Figure 3). This difference is stronger in ARPEGE

(Figure 3a) and ECHAM 4 (Figure 3b) and weaker for ECHAM 3 (Figure 3c) and GISS (Figure 3d). In ARPEGE and GISS (Figures 3a and 3d) the highest intensity of the monsoon flow is also shifted toward the central and eastern Sudan-Sahel belt, compared to the ERA-40.

[16] The mean seasonal evolution of the 200 hPa zonal wind component (850 hPa wind modulus) averaged over the box 20°W to 20°E ; 3° – 13°N (same limits as *Garric et al.* [2002]) is displayed in Figure 4a (Figure 4b). TEJ peaks clearly in July–August in concomitance with the Asian-African northern monsoon system; overall, the seasonal phase is well simulated, but the differences regarding wind speed compared to the ERA-40, already stressed for August (Figure 2), are also observed for the whole summer season (Figure 4a). The observed seasonal evolution in low levels is characterized by a weak but robust strengthening of the eastward wind component: The weak southerlies in May are clearly replaced by a southwesterly circulation peaking in July–August. In October (Figure 4b) the northeasterly Harmattan is reinstalled in association with the monsoon withdrawal. This seasonal evolution appears well simulated

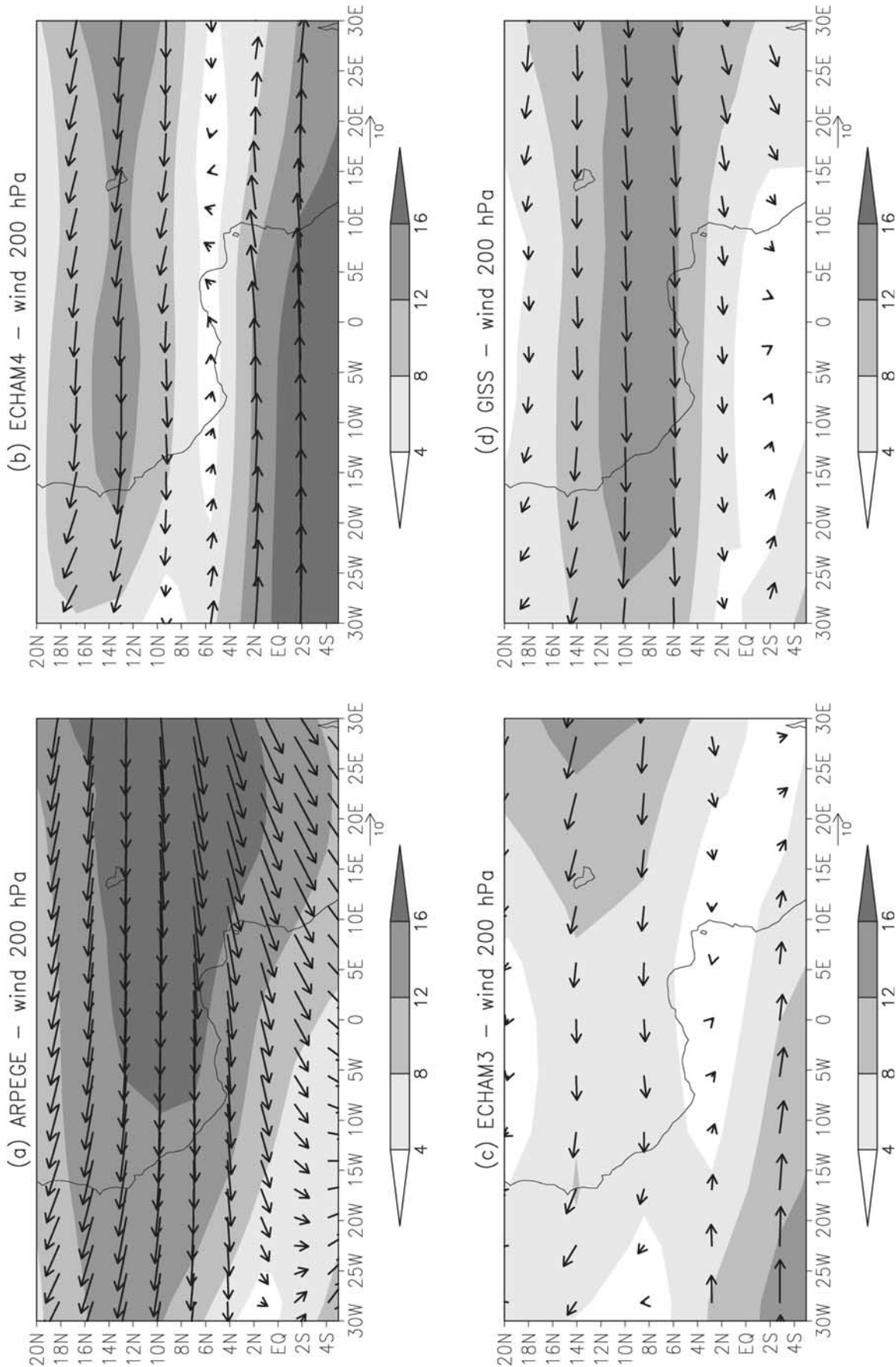


Figure 2. Mean wind (arrows) and modulus of the wind (shading) in m/s in August at 200 hPa for (a) ARPEGE (period 1948–1997), (b) ECHAM 4 (period 1961–1994), (c) ECHAM 3 (period 1950–1994), and (d) GISS (period 1951–1998). The vector scale is indicated at the bottom of each panel.

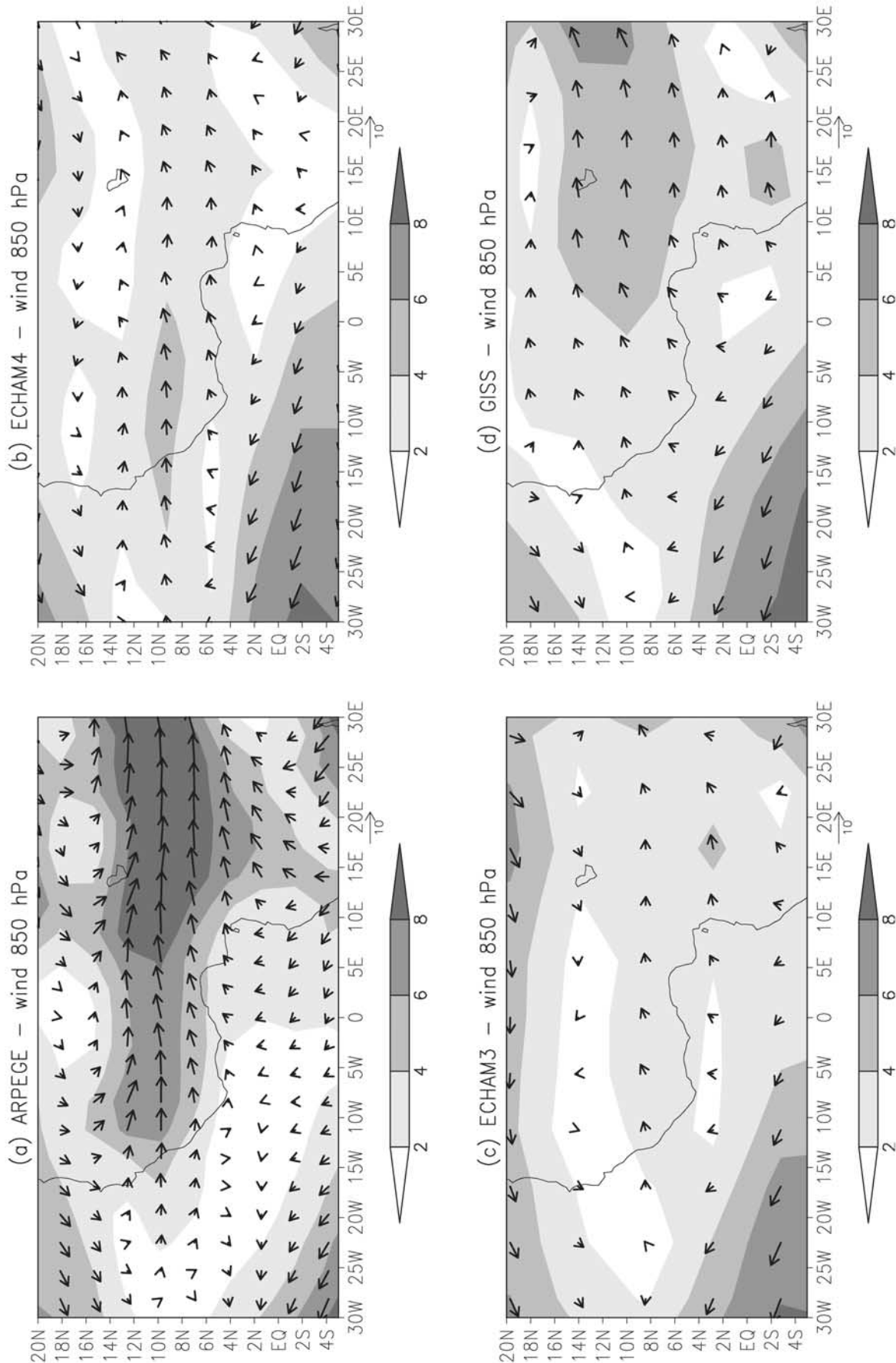


Figure 3. Mean wind (arrows) and modulus of the wind (shading) in m/s in August at 850 hPa for (a) ARPEGE (period 1948–1997), (b) ECHAM 4 (period 1961–1994), (c) ECHAM 3 (period 1950–1994), and (d) GISS (period 1951–1998). The vector scale is indicated at the bottom of each panel.

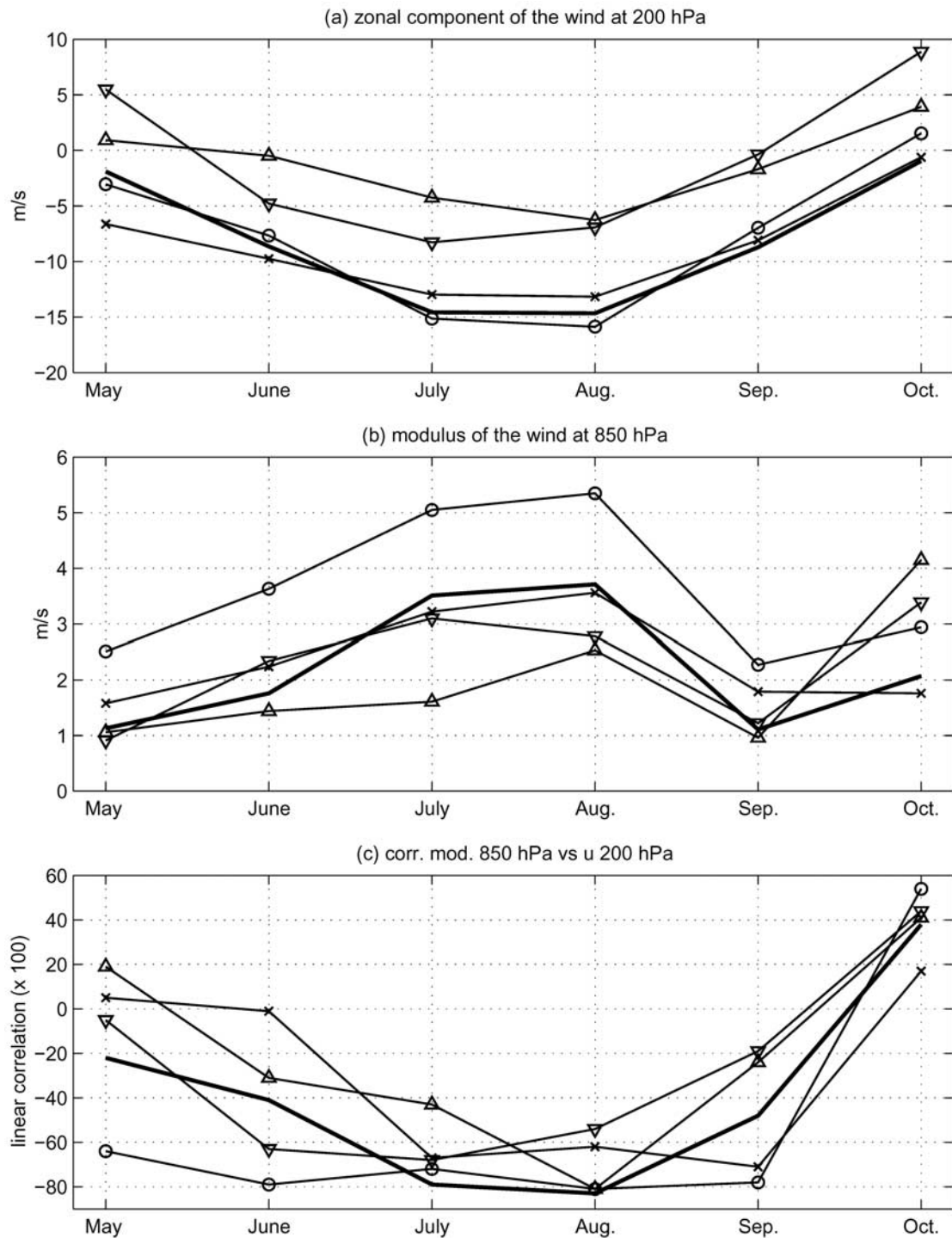


Figure 4. Monthly mean evolution of (a) the zonal component of the wind at 200 hPa, (b) the modulus of the mean wind at 850 hPa, averaged over 20°W to 20°E , 3° – 13°N , and (c) their correlation ($\times 100$) in ERA-40 (bold line), ARPEGE (line with circles), ECHAM 4 (line with downward pointing triangles), ECHAM 3 (line with upward pointing triangles) and GISS (line with crosses). Mean values and correlation coefficients are computed over the 1961–1994 period.

Table 1. Mean Speed of the Wind (Standard Deviation of the Wind) at 850 hPa (MOD850) and of the Zonal Component of the Wind at 200 hPa (U200) for ERA-40, NCEP-1, and Each AGCM (Mean of Available Runs) in the 1961–1994 (July–September) Period Averaged Over 20°W to 20°E, 3°–13°N, As Well As Linear Correlations ($\times 100$) Between MOD850 and U200

	MOD850, m/s	U200, m/s	Correlation MOD850 Versus U200
ERA-40	+2.8 (0.6)	–12.7 (2.0)	–84 ^a
NCEP-1	+2.6 (2.1)	–13.7 (2.7)	–82 ^a
ARPEGE	+4.2 (0.8)	–12.7 (1.9)	–80 ^a (–77 ^b)
ECHAM 4	+2.4 (0.4)	–5.2 (1.7)	–59 ^a (–58 ^b)
ECHAM 3	+1.7 (0.4)	–4.1 (2.4)	–66 ^a (–57 ^b)
GISS	+2.9 (0.4)	–11.4 (0.9)	–81 ^a (–56 ^b)

^aSignificant values at the one-sided 0.01 “random-phase” test [Janicot *et al.*, 1996, 2001; Ebisuzaki, 1997]. The values are computed over the 1961–1994 time period, and for each AGCM the ensemble mean (concatenated runs) is displayed.

overall; however, several topics have to be pointed out: In the selected regional box, the monsoon flow intensity seems too strong in ARPEGE (Figure 4b), and the direction of the flow is also too westerly (not shown) and too weak in the remaining models (Figure 4b). So if the AGCMs are able to simulate a monsoonal circulation over West Africa that is similar to ERA-40, especially ARPEGE, the monsoon flow is weaker in ECHAM 3 and ECHAM 4 than in ERA-40 and overall the TEJ axis is shifted northward compared to ERA-40.

[17] Various studies [Webster and Yang, 1992; Fontaine *et al.*, 1995; Moron *et al.*, 1995; Goswami *et al.*, 1999] have indicated that the low-level and upper level winds are inversely related in the tropics mainly over the monsoonal area. In particular, a positive anomaly of the wind modulus at 850 hPa (i.e., strengthening and/or deepening of the monsoon flow) is usually associated with a negative anomaly of the zonal wind component at 200 hPa (i.e., strengthening of the TEJ) and vice-versa. The monthly correlation between wind speed of the zonal component at 200 hPa and wind speed at 850 hPa is displayed in Figure 4c, and the mean seasonal value in July–September (JAS) is shown in Table 1 (fourth column). The negative correlations are always significant at the one-sided 0.05 level in July–August and then decrease in September (mainly in ECHAM 3–4). The signs of the correlations in Figure 4c change in October in relationship to the disappearance of the TEJ in the upper troposphere and the low-level monsoon flow. Note that correlations between MOD850 and U200 are quite similar for the ensemble mean and the concatenated runs for ARPEGE and ECHAM 4, but quite different for ECHAM 3 and mainly GISS. The inverse relationship between upper and lower levels of the WAM circulation is thus stable for the first two AGCMs and noisier for GISS, with correlations for individual runs varying from –0.32 (not significant) to –0.65 (unless stated, the correlations indicated in the text are significant at the 0.01 level according to a random-phase test, where 10,000 random time series with the same spectral power, but random phases, are correlated [Janicot *et al.*, 1996; Ebisuzaki, 1997]).

[18] We define, then, a dynamical index, called the West African Monsoon Index (WAMI), that stands for the monsoon circulation in terms of both vertical and horizontal internal coherency: the vertical shear is estimated from the

difference between the 850 hPa wind modulus (MOD850) and the 200 hPa zonal wind component (U200), averaged from 20°W to 20°E and from 3°N to 13°N in exactly the same way as done by Garric *et al.* [2002]. Notice that the interannual variability of WAMI is dominated by U200: Its standard deviation is 2.5–6 times greater than MOD850 (Table 1).

4. Interannual Variability and Teleconnections With SST

4.1. Interannual Variability of WAMI

[19] Figure 5a displays the interannual evolution of WAMI averaged over the northern summer (JAS) as estimated through ERA-40 (bold line with squares) and NCEP-I (solid thin line) reanalyses. Note that in NCEP (but not in ERA-40), WAMI is characterized by a strong decrease between 1966 and 1967 (Figure 5a), mainly through the modulus of the wind at 850 hPa (not shown; see standard deviation of MOD850 in NCEP-1 in Table 1), due to changes in the assimilation procedure in NCEP data [Poccard *et al.*, 2000; Camberlin *et al.*, 2001; Janicot *et al.*, 2001]. After 1967, by contrast, ERA-40 and NCEP-I WAMI estimates are very close ($r = 0.72$) and highly similar after 1979 because of the efficient assimilation of satellite data both in ERA-40 and NCEP-I. When WAMI is computed from the “Oort” data set, which includes just a statistical Cressman algorithm to interpolate station values onto a regular grid [Oort, 1978; Oort and Liu, 1993; Moron *et al.*, 2001], its values are more correlated with ERA-40 ($r = 0.86$) than with NCEP-I ($r = 0.60$) over the common period (1963–1989), but over the period 1968–1989 they are quite similar ($r = \sim 0.86$ with the two reanalyses). In the following, the wind data will be issued from ERA-40 whereas the discrepancy between ERA-40 and NCEP-I (mostly before 1968, then in 1973 and 1977–1978; see Figure 5a) will give us a rough estimate of the uncertainty in the reanalyzed WAMI, used here as a surrogate for the observations. This allows us to fix an upper limit to the skill that could be reached by any AGCM.

[20] Figure 5b also shows WAMI calculated for the four AGCMs (markers) and ERA-40 (solid bold line). Over the 1961–1994 common period, skill is highly significant (correlation between reanalyzed and simulated (equals ensemble mean of each AGCM) WAMI equals 0.58, 0.64, 0.56 and 0.51 for ARPEGE, ECHAM 4, ECHAM 3 and GISS, respectively). It should be emphasized here that the amount of SST-forced variance (computed with the algorithm of Rowell *et al.* [1995]) equals 58%, 34%, 55% and 51% for ARPEGE, ECHAM 4, ECHAM 3 and GISS, respectively, over the 1961–1994 period. The low value for ECHAM 4 is partly attributable to the small number of available runs, since the external variance, computed with ANOVA methods as done here, usually increases with the number of available runs [Gualdi *et al.*, 1999]. Thus the skill is not very far from the highest reachable value, if ERA-40 is considered as a good surrogate for observation, since AGCM is just able to correctly fit the SST-forced variance. Moreover, the skill is largely higher than that for Sahelian rainfall [Sud and Lau, 1996; Sperber and Palmer, 1996; Moron *et al.*, 2003]. Garric *et al.* [2002] found a slightly higher skill for WAMI with ARPEGE ($r = 0.71$) but

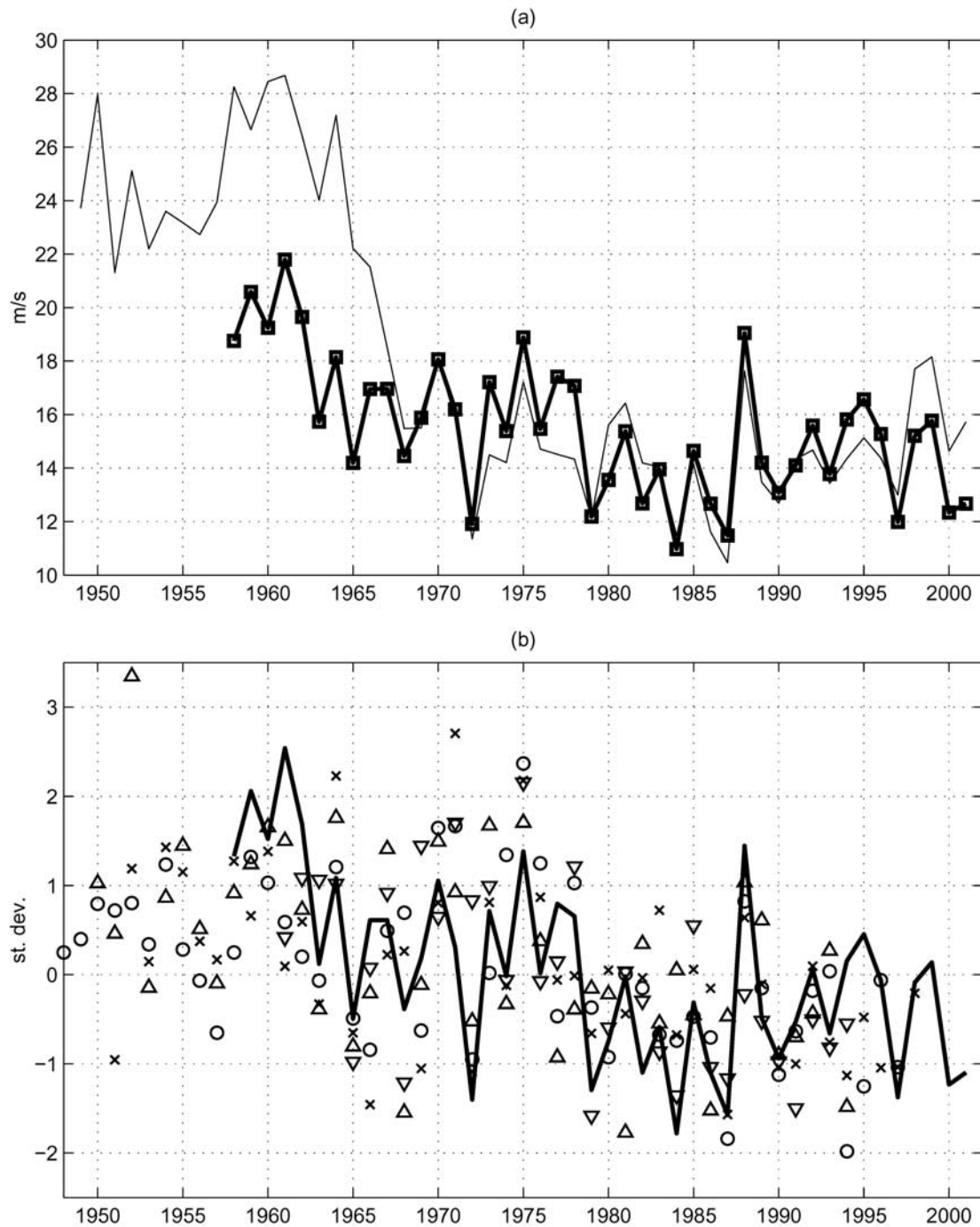


Figure 5. (a) WAMI (modulus of the wind at 850 hPa minus the zonal component wind at 200 hPa) in m/s computed from ERA-40 (bold line with squares) and NCEP-I (thin line). (b) WAMI from ERA-40 (bold line) and simulated by ARPEGE (circles), ECHAM 4 (downward pointing triangles), ECHAM 3 (upward pointing triangles), and GISS (crosses). The simulated WAMI are the mean ensemble of all available runs for each AGCM. All time series in Figure 5b are standardized to zero mean and unit variance over the common period 1961–1994.

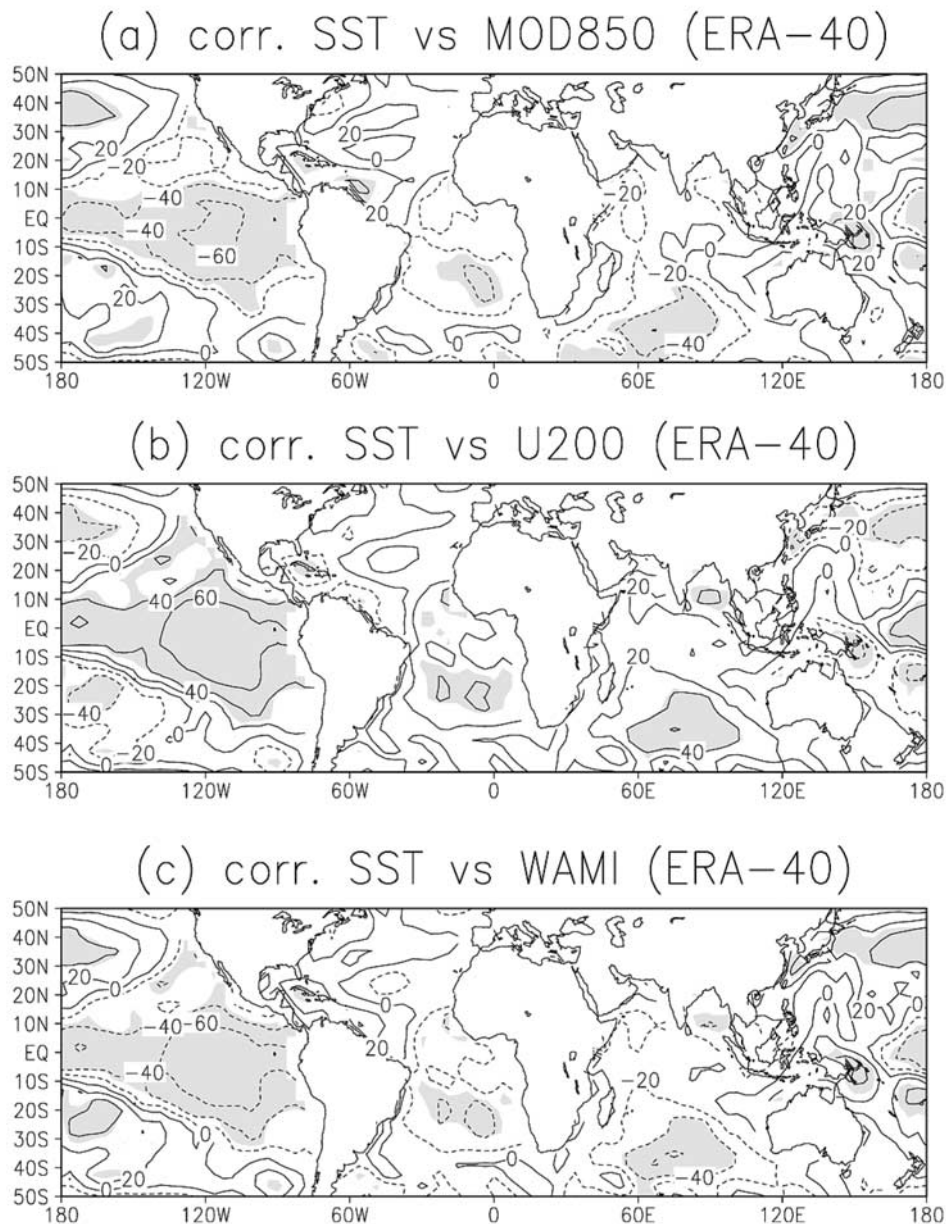


Figure 6. Correlation ($\times 100$) between SST and (a) the modulus of the wind at 850 hPa, (b) the zonal component of the wind at 200 hPa, and (c) WAMI computed over the window 20°W to 20°E , 3° – 13°N (from ERA-40). Shading indicates significant values at the two-sided 0.1 level according to a random-phase test.

over a shorter period than here (1979–1993) and with a different integration scheme. The skill equals 0.74 here over the 1979–1993 period for ARPEGE. Note that the correlation between the ensemble of the four AGCMs' mean and ERA-40 equals 0.68 over the common period 1961–1994.

4.2. Teleconnections With SST at Seasonal Scale

[21] Figure 6 displays, for the JAS season, the observed SST field–WAMI (and its components) relationship in terms of correlation coefficients. The pattern in Figure 6 emphasizes the role of tropical Pacific forcing and, namely, of the ENSO phenomenon: Warm (cold) SST anomalies (SSTA hereafter) in the central and eastern equatorial

Pacific are associated with a weaker (stronger) than normal West African monsoon [e.g., Palmer *et al.*, 1992; Moron *et al.*, 1995; Rowell *et al.*, 1995; Janicot *et al.*, 1996; Rowell, 2001]. The ENSO–WAMI link results from perturbations in the E–W quasi-divergent cells [Janicot *et al.*, 1998, 2001; Rowell, 2001]: Warm (cold) ENSO events are associated with a weakened (strengthened) TEJ (Figure 6b) and anomalous subsiding (ascending) motions over the whole boreal monsoon sector. The ITCZ tends also to be shifted southward during warm events [Rowell, 2001]. The Atlantic signal is weaker even at 850 hPa (Figure 6a).

[22] To check the consistency between the observed and simulated teleconnections structures [Sperber and Palmer,

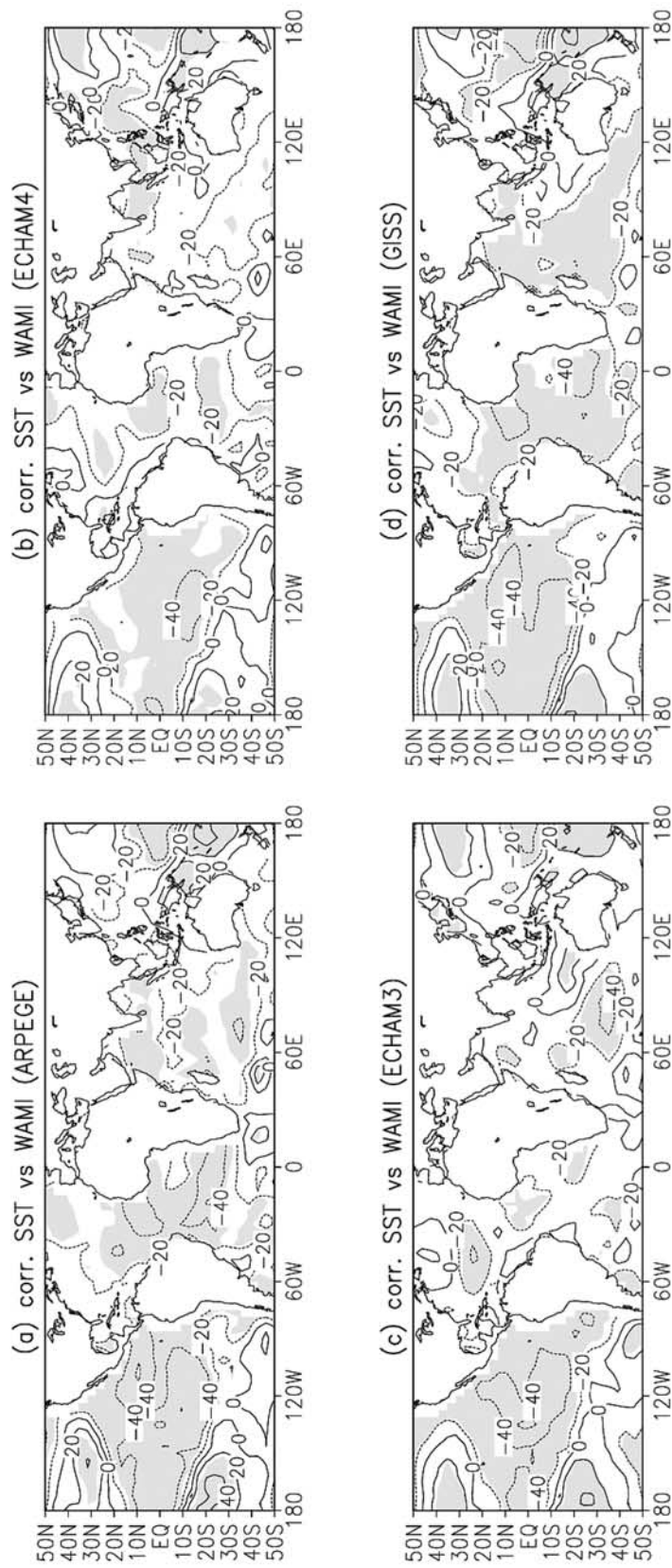


Figure 7. Same as Figure 6c except for (a) ARPEGE, (b) ECHAM 4, (c) ECHAM 3, and (d) GISS. For each AGCM, correlations are computed using the concatenated individual runs. Shading indicates significant values at the two-sided 0.1 level according to a random-phase test.

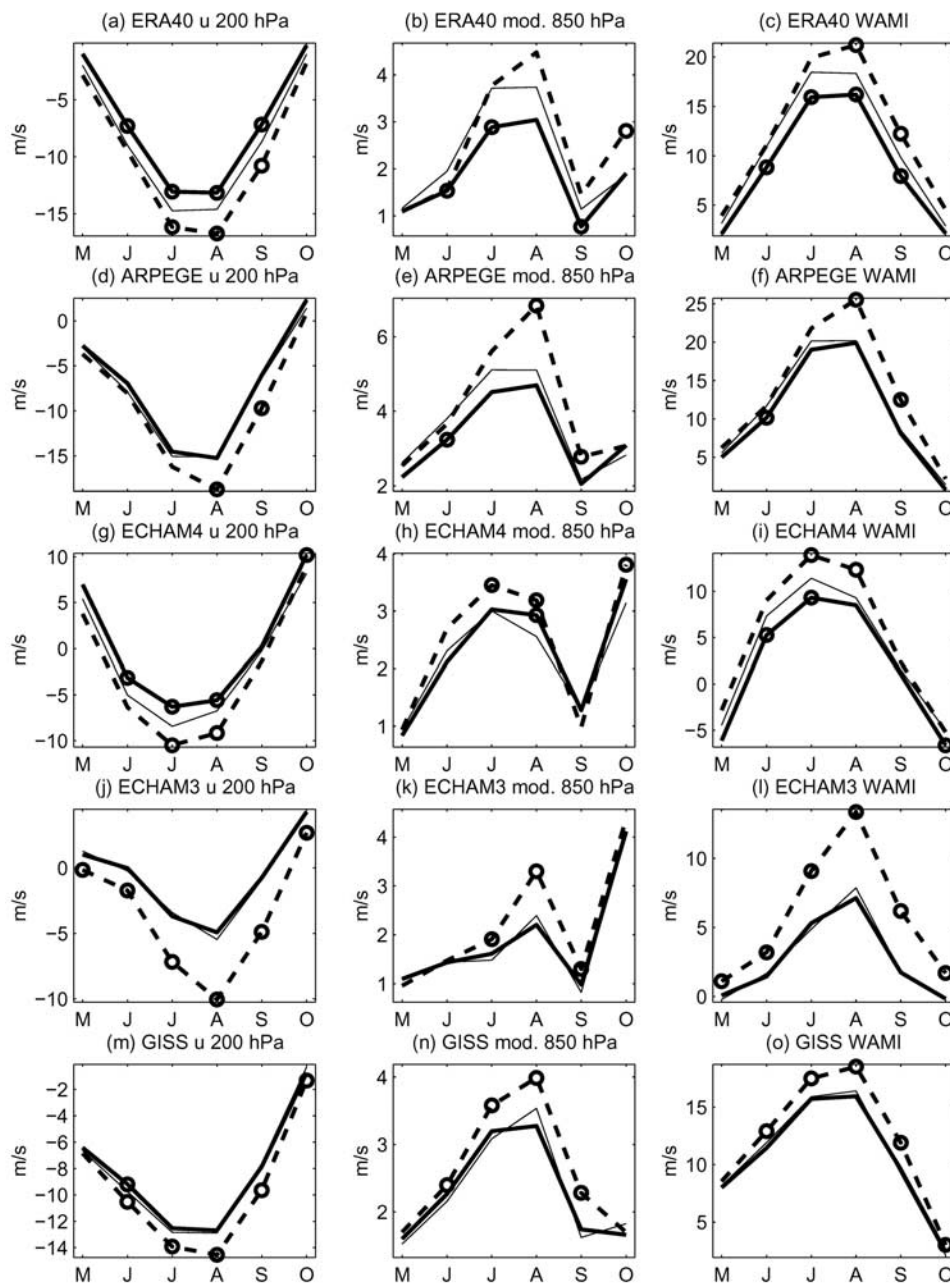


Figure 8. Mean monthly wind values during warm (bold solid line), cold (bold dashed line) and neutral (thin solid line) in m/s for the modulus of the wind at 850 hPa (second column), the zonal component of the wind at 200 hPa (first column) and WAMI (third column) from (a–c) ERA-40, (d–f) ARPEGE, (g–i) ECHAM 4, (j–l) ECHAM 3 and (m–o) GISS. The values for each AGCM are the mean of the available runs, and the circles indicate significant anomalies at the two-sided 90% level according to a Student t test (H_0 : the mean anomaly of the warm/cold years equals the mean anomaly of the neutral years).

1996], each simulated WAMI is correlated with the SST field (Figure 7). Correlations in Figure 7 are computed using the concatenated individual runs from each AGCM rather than the ensemble means. This allows a fair comparison with ERA-40, for which only one realization is available. The modeled teleconnections with SST (Figure 7) match quite accurately those estimated from ERA-40 (Figure 6c) but with a weaker amplitude. As in observations, the major forcing on simulated WAMI is partially related to ENSO [Janicot *et al.*, 2001; Rowell *et al.*, 1995; Rowell, 2001]: A

weak (strong) monsoon is associated with warm (cold) ENSO and also warm (cold) SSTA in the SW Indian Ocean and the whole tropical Atlantic. However, compared to ERA-40 (Figure 6c), the best correlations over the eastern equatorial Pacific (located near 120°W and 7°–10°S in the observations, Figure 6c) weaken (mainly in ECHAM 3 and ECHAM 4, because of a southward shift of the highest values, Figures 7b and 7c). The “rather good” observed/simulated likeness in teleconnections points out AGCMs’ ability to simulate dynamical links of large scale. Each

Table 2. WAMI Composites in Standardized Anomalies for the Warm and Cold ENSO Years (See Text) for Each AGCM Ensemble Mean and ERA-40 (Zero Mean and Unit Variance) Along With in Parentheses the Number of Years With the Same Anomaly Polarity

	Warm ENSO (9 Years)	Cold ENSO (7 Years)
ERA-40	-0.8 ^a (8)	+0.9 ^a (7)
ARPEGE	-0.5 (7)	+1.2 ^b (7)
ECHAM 4	-0.7 ^c (8)	+1.0 ^b (6)
ECHAM 3	-0.4 (6)	+1.4 ^b (7)
GISS	-0.4 (7)	+1.4 ^b (7)

^aSignificant values at the two-sided 0.1 Student *t* test.

^bSignificant values at the two-sided 0.02 Student *t* test.

^cSignificant values at the two-sided 0.2 Student *t* test (H0: the mean of

AGCM also exhibits a clear regional SST forcing over the tropical Atlantic (mainly its southern and equatorial parts) and the western Indian Ocean (Figure 7), where cold (warm) SSTAs are associated with an anomalously strong (weak) West African monsoon [Hastenrath, 1990; Fontaine and Bigot, 1993; Rowell *et al.*, 1995; Giannini *et al.*, 2003]. There are some differences among the four AGCMs (Figure 7). For example, the relationships between WAMI and the southern Atlantic Ocean appear to be stronger for ARPEGE (Figure 7a) and GISS (Figure 7d) than for ECHAM 4 (Figure 7b) and ECHAM 3 (Figure 7c). However, these differences could be associated with sampling variability, and it is not reasonable to speculate further on this issue just with the evidence presented here.

4.3. ENSO Impact at Monthly and Seasonal Scales

[23] The relationship between WAMI and its components and the tropical Pacific is further investigated since the central and eastern basins seem to provide the main SST forcing (Figure 7). The seasonal phase and intensity of WAMI and its components during major ENSO are displayed in Figure 8, and the mean standardized anomaly of WAMI in JAS is displayed in Table 2. The cold (warm) events are defined from the multivariate ENSO index defined by Wolter and Timlin [1998]: The July–August or August–September bimonths ranked in the 1–2 (6–7) categories (see Table 1 of Wolter and Timlin [1998]) define here the cold (warm) years, i.e., 1964, 1967, 1970, 1971, 1973, 1975, 1988 (1965, 1972, 1976, 1982, 1983, 1986, 1987, 1991, 1993, respectively). The 18 remaining years are said to be “neutral.” In ERA-40 (Figures 8a–8c and Table 2) the cold (warm) ENSO events are associated with stronger (weaker) flows without any significant phase shift. Regarding simulations, anomalies are much more marked (and significant) during cold events (Figures 8d–8o), mainly consisting in a significant acceleration of the TEJ in July–August (August–September in ARPEGE, Figure 8d) and of the monsoon flow from July to September. The mean anomalies during warm events are almost equivalent to those observed during “neutral” years except for ECHAM 4 (Table 2). Nevertheless, the overall monsoon is usually anomalously weak during warm ENSO events (Table 2). Last, as in ERA-40, the seasonal phase of simulated WAMI and its component is not significantly modified during warm/cold events

(Figure 8). In summary, there is a stronger asymmetry between simulated WAMI during warm and cold ENSO extremes than between reanalyzed WAMI during these events.

5. Yearly Analysis of Reproducibility and Skill of WAMI in the Multimodel Ensemble

[24] The above sections indicated that the mean teleconnections linking the observed WAMI to SST are correctly simulated, mainly if we consider the teleconnections with the tropical Pacific and the southern and equatorial Atlantic (Figures 6 and 7). The objective is now to assess the reproducibility and skill of WAMI on a yearly basis using a probabilistic approach. Figure 9a (Figure 9b) displays the cumulative distribution function (CDF) for 1974 (1975) and the “climatological” one. Note that the “climatology” is almost identical in both cases and broadly Gaussian. The CDF of the 21 runs in 1974 is very close to the “climatology” one (Figure 9a). By contrast, in 1975, the 21 runs are all strongly positive and visually very far from the “climatology,” suggesting a strong forcing of the SST during that year (Figure 9b). KS for all years is displayed on Figure 9c with the one-sided 0.1, 0.05 and 0.01 levels of significance estimated with a Monte Carlo procedure (1000 random samples of 21 runs coming from different years are compared with the remaining 693 runs). The reproducibility is usually higher during cold than during warm ENSO years (Figure 9c). KS could be also moderate to strong during neutral years (as in 1961, 1966, 1980, 1984, 1990 and 1994). The better reproducibility observed during cold ENSO years is not associated with a smaller spread between runs or AGCMs than during the warm ENSO or neutral years (not shown). So in cold ENSO years, the noise associated with the different internal atmospheric processes between runs and AGCMs is not significantly reduced. Their better reproducibility is mainly due to a stronger amplitude of simulated anomalies (Table 2). KS, computed with 1000 samples of 12 members considering 3 runs from each AGCM, yields almost the same results (not shown).

[25] The interannual variability of skill is assessed through RPSS (Figure 9d). An important interannual variability of the skill is observed even when considering other thresholds or a different number of categories (this yields rather similar results). In general, RPSS is always above 50% during the cold ENSO years, which indicates a strong improvement versus climatology. Regarding the warm ENSO and neutral years (Figure 9d), larger spread is observed in RPSS values. Simulated WAMI is too strong relative to ERA-40 in 5 warm ENSO years (i.e., 1972, 1976, 1982, 1983, 1993). This is mainly due to ECHAM 3 and ECHAM 4 (1972), ARPEGE and GISS (1976), all AGCM (1982), GISS (1983) and ECHAM 3 and ARPEGE (1993) (Figure 5b). Note also that ARPEGE and GISS are rather skillful in simulating reanalyzed WAMI during the warm ENSO event of 1997 (Figure 5b). RPSS has been also computed on 1000 samples of 12 members considering 3 runs from each AGCM and yielded almost the same results (not shown). The strong variability of skill in warm ENSO events does not necessarily reflect a deterministic signal but

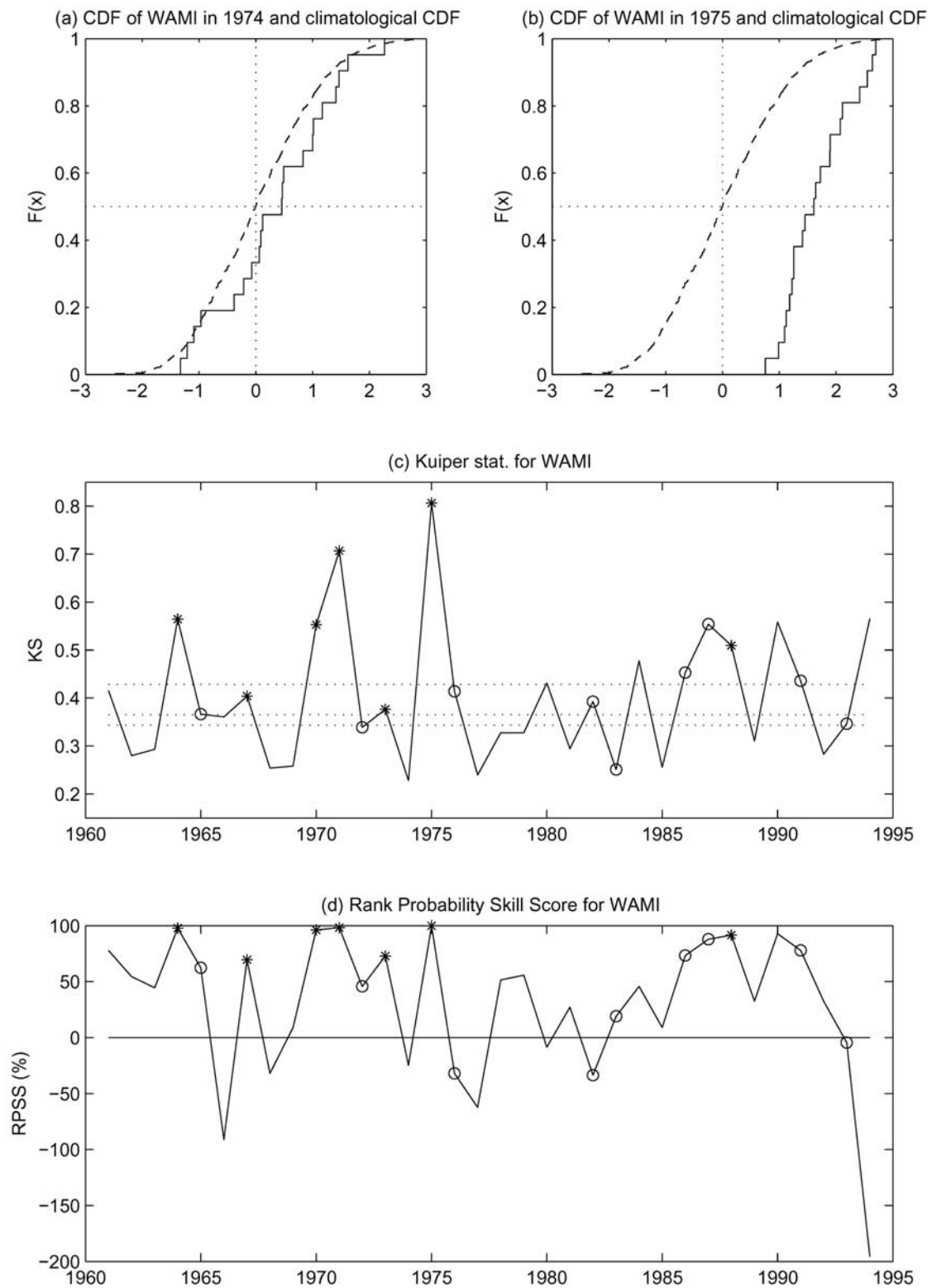


Figure 9. Cumulative distribution function for WAMI (solid lines) and the remaining years (dashed lines) in (a) 1974 and (b) 1975. Yearly KS score for (c) WAMI, with the one-sided 0.1, 0.05 and 0.01 level of significance (dotted lines) estimated through a Monte Carlo procedure (see text). (d) Ranked probability skill score (in percent) for WAMI; Stars (circles) indicate the cold (warm) ENSO events.

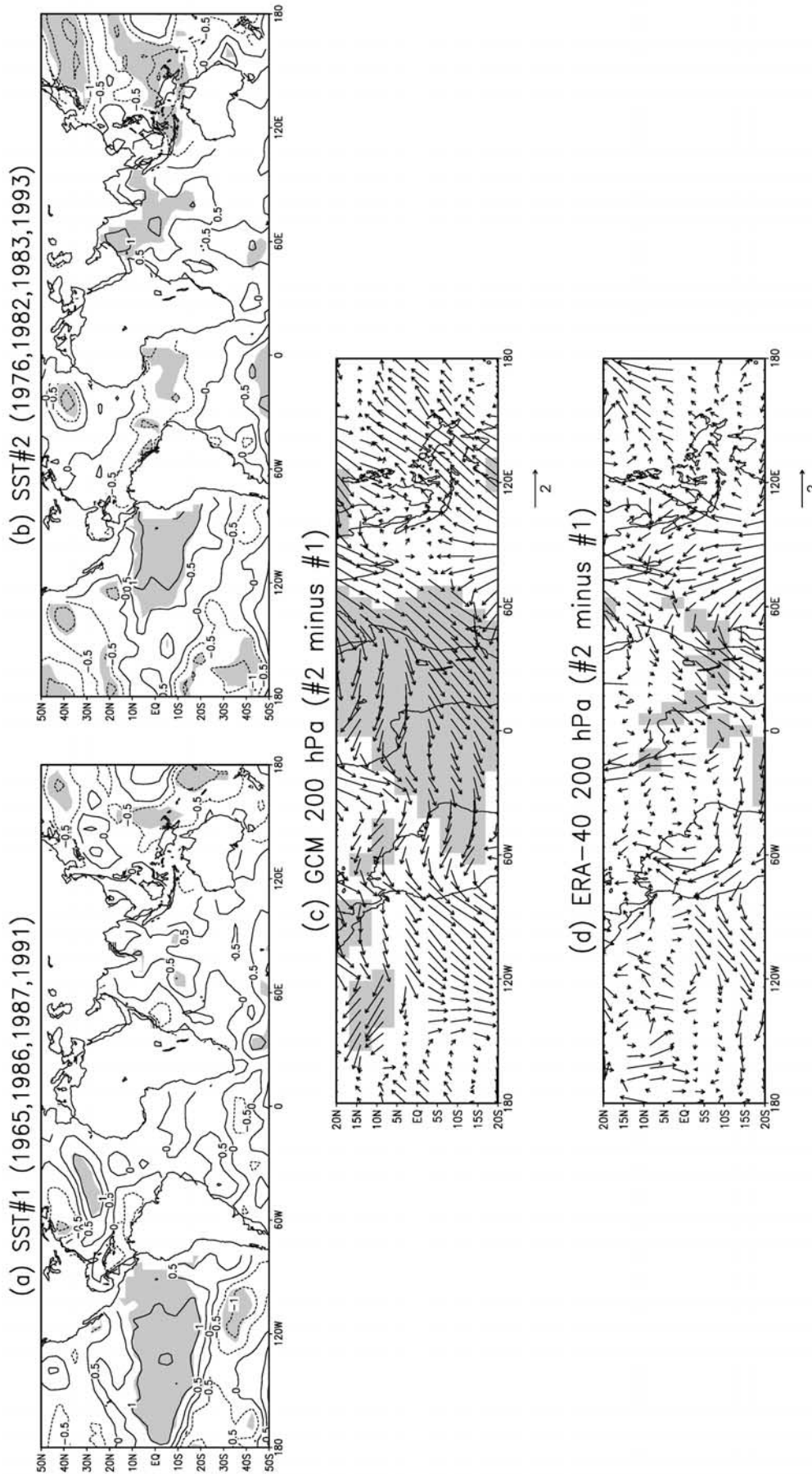


Figure 10. (a) Mean SSTA for the warm ENSO events of 1965, 1986, 1987 and 1991. (b) Mean SSTA for the warm ENSO events of 1976, 1982, 1983 and 1993 (shading indicates significant values at the two-sided 0.1 level according to a Student's t test (H0: the mean of the warm ENSO sample equals the mean of the neutral years in the 1961–1994 period)). (c) Difference between the 200 hPa wind anomaly simulated in (1976, 1982, 1983, 1993) minus the one simulated in (1965, 1986, 1987, 1991). The AGCM mean is the mean of the four AGCMs (the AGCM mean is standardized to zero mean and the unit variance on the 1961–1994 period). The vector scale is indicated at the bottom of the panel. (d) Difference between the 200 hPa wind anomaly simulated in (1976, 1982, 1983, 1993) minus the one simulated in (1965, 1986, 1987, 1991) in ERA-40 (the ERA-40 mean is standardized to zero mean and unit variance on the 1961–1994 period). In Figures 10c and 10d, shading indicates significant values at the two-sided 0.1 level according to a Student's t test (H0: the mean of both samples is equal). The vector scale is indicated at the bottom of the figure.

could be associated with sampling variations. Nevertheless, this is consistent with the result listed in section 4.

[26] It is beyond the scope of this paper to explain the differences observed among the warm ENSO events, but a hypothesis can be put forward. Figure 10 displays the SST anomalies field for the skillful warm ENSO events (i.e., those with RPSS > 50%, suggesting a strong improvement relative to climatology, Figure 9d) (Figure 10a) and the unskillful warm ENSO events (i.e., those where RPSS is close to zero or negative, Figure 9d) (Figure 10b). The skillful ENSO events (Figure 10a) are mainly characterized by warm SSTAs over the central-eastern tropical Pacific and usually over the subtropical North Atlantic, promoting then a negative anomaly of WAMI in AGCMs (Figure 7). By comparison, the unskillful ENSO events (Figure 10b) are characterized by warm SSTAs in the tropical Pacific but only significantly eastward of 140°W. More important, they are also associated with a significant cooling over the equatorial Atlantic and western Pacific Ocean and a significant warming in the tropical Indian Ocean. The cold SSTAs over the equatorial Atlantic propagate deep into the Gulf of Guinea, which could induce a positive WAMI anomaly, as shown mainly in ARPEGE and GISS simulations (Figures 7a and 7d). The two last panels show the differences between the two categories of warm ENSO events within the AGCMs (mean of each AGCM) (Figure 10c) and in ERA-40 regarding the 200 hPa field (Figure 10d). It is striking that over the whole tropical belt, differences are strong within the AGCMs (and statistically significant over and around Africa) but quite weak in ERA-40. In particular, the models simulate a strong northeasterly anomaly across North Africa during the unskillful warm events (Figure 10c), consistent with a too strong WAMI. So it seems that when an AGCM runs in forced mode (that is to say, its atmospheric response depends only on the SST forcing), it is oversensitive to the particular SSTA pattern displayed in Figure 10b; this is not attested in the ERA-40 reanalyses since they incorporate the available observations through the assimilation process (Figure 10d). It remains, however, necessary to examine whether the bias registered in AGCMs (regarding ERA-40) is associated more with the whole tropical part of the pattern than with any particular oceanic basin.

6. Summary and Conclusion

[27] We have analyzed the behavior of 21 runs coming from four AGCMs (ECHAM 3, ECHAM 4, ARPEGE and GISS) in simulating and predicting the seasonal mean and interannual variability of the West African monsoon (WAM) dynamics and compared these models with ERA-40 reanalyses.

[28] The results show a rather good AGCM ability (albeit depending on the model) to simulate monsoonal circulation over West Africa that is similar to ERA-40 (Figure 1) in terms of both intensity and seasonal evolution, with, however, a weaker southern wind component at low levels around 10°N (Figure 3) and a Tropical Easterly Jet (TEJ) axis shifted northward compared to the ERA-40 (Figure 2). The TEJ is also weaker in ECHAM 3 and ECHAM 4 than in ERA-40 (Figures 2b and 2c). The particular vertical wind structure observed above the West African monsoon (i.e.,

the connection between the low-level and upper level flows through divergent circulation and moist convection) is well simulated by the four AGCMs (Figure 4c and Table 1) and allowed us to define a WAM dynamical index (WAMI). This index has been defined by the difference between the wind modulus at 850 hPa just at the summit of the wet monsoon flux and the zonal component of the TEJ (Figure 5). This index is dominated by the interannual variability of the TEJ (Table 1).

[29] The interannual variability of the West African monsoon has been analyzed in terms of these three indices. The simulation of the interannual variability of the wind indices is not too strongly model dependent. It can therefore be considered mainly as a deterministic result from the SST forcing. As in ERA-40 (Figure 6), a weak (strong) monsoon is associated with warm (cold) ENSO-like episodes along with warm (cold) SSTA in the SW Indian Ocean and the southern and equatorial parts of the tropical Atlantic (Figure 7). This “rather good” reanalyzed/simulated likeness in teleconnections points out the AGCMs’ ability to simulate dynamical links at least at regional scale. The four AGCMs also seem oversensitive to western tropical Pacific SST (Figure 7). On a yearly basis, the Kuiper statistic and the rank probability skill score were used to estimate the reproducibility and the skill of the 21 runs in a probabilistic way. The results reveal an asymmetry of the simulated WAMI in warm and cold ENSO years (Figure 8), whereas there is little difference between the magnitudes of the reanalyzed WAMI in warm/cold years. The reproducibility and skill (Figure 9) in cold ENSO years are higher than in years registering warm episodes. This is mainly due to stronger amplitudes of anomalies in the models (Table 2). So, during warm events, WAMI appears less predictable and less skillful than during cold occurrences. It remains to be understood if these errors come from a particular SST pattern and/or from other factors not properly considered by these experiments. It seems that the composite of the unskillful warm ENSO years (i.e., 1976, 1982, 1983, 1993) is characterized by a quadrupole SSTA pattern along the equatorial belt with warm (cold) SSTA over the eastern Pacific and Indian Ocean (Atlantic Ocean and western Pacific) (Figure 10). Outside the extreme ENSO events, the SST forcing can also be significant, as in 1961, 1966, 1980, 1984, 1990 or 1994 (Figure 9c), but the skill could be very low during such years (as in 1966 and 1994), pointing out systematic errors of the AGCM in the relationships between SST and WAM and/or strong influence of any forcing not included in these experiments (Figure 9d).

[30] Future works should investigate several questions: First, these results need to be checked with a larger sample of AGCMs including more runs since it is clear that the yearly analysis performed here is biased by sampling variations. The evaluation of KS and RPSS is also biased by the different number of runs available for each AGCM. The asymmetry between simulated WAMI during warm and cold ENSO events and the systematic errors observed here during particular warm ENSO events (mainly 1976, 1982, 1983, 1993) should be carefully checked and, if real, explained. It is possible that systematic biases in mean wind field, even outside West Africa, modify the teleconnection between WAMI and its component and SST. Second, additional studies are also needed to construct and evaluate

statistico-dynamical forecasting schemes for Sahelian rainfall since WAMI (1) is strongly related to Sahelian rainfall index (SRI) and (2) seems potentially predictable and skillful from SST forcing (Figure 7 and Table 2), even if predictability and skill are yearly variable and seem strongest during the cold ENSO events (Figure 9 and Table 2). In particular, the skill of WAMI largely outperforms the SRI one (the correlations between observed and simulated SRI ensemble mean time series over 1961–1994 range between 0.10 (ECHAM 4) and 0.47 (ECHAM 3) and decreases below 0.20 (not significant) for the four AGCMs when the interannual variability with frequencies higher than 1/8 cycle per year is considered). Various analyses of DEMETER runs [Palmer *et al.*, 2004] would help to investigate such future work.

[31] **Acknowledgments.** Parts of this study were helped by the ECLAT/PNEDC 358085 and ESCALAO/PNRH 262085 contracts. Runs of ECHAM 3 and ECHAM 4 come from the EC contract DICE-EV5V-CT94-0538 project. Runs from ARPEGE were kindly supplied by L. Terray of CERFACS. J. Hansen kindly provided us with references and preprints about GISS runs. ECMWF ERA-40 data used in this study have been obtained from the ECMWF data server. NCEP data and runs from GISS2000 were downloaded from the IRI website (<http://ingrid.ldgo.columbia>). Discussions with H. Douville (CNRM) on land surface schemes of ARPEGE AGCMs were also fruitful during the development of this work. We thank also A. Robertson (IRI, New York) and J. Swann (Birbeck College, London) for their careful reading.

References

- Anderson, J. L., and W. F. Stern (1996), Evaluating the potential predictability utility of ensemble forecasts, *J. Clim.*, *9*, 260–269.
- Camberlin, P., S. Janicot, and I. Poccard (2001), Seasonality and atmospheric dynamics of the teleconnections between African rainfall and tropical ocean surface temperature: Atlantic vs. ENSO, *Int. J. Climatol.*, *21*, 973–1005.
- Cassou, C., and L. Terray (2001), Influence of tropical and extratropical SST on inter-annual atmospheric variability over the North Atlantic, *J. Clim.*, *14*, 4265–4280.
- Cherchi, A., and A. Navarra (2003), Reproducibility and predictability of the Asian summer monsoon in the ECHAM4-GCM, *Clim. Dyn.*, *20*, 365–379.
- Déqué, M., C. Drevet, A. Braun, and D. Cariolle (1994), The ARPEGE/IFS atmosphere model: A contribution to the French community climate modeling, *Clim. Dyn.*, *10*, 249–266.
- Deutsches Klimarechenzentrum (DKRZ) (1993), The ECHAM3 atmospheric general circulation model, *MPI Rep. 6*, 195 pp., Hamburg, Germany.
- Doblas-Reyes, F., M. Déqué, and J. P. Piedelièvre (2000), Multi-model spread and probabilistic seasonal forecasts in PROVOST, *Q. J. R. Meteorol. Soc.*, *126*, 2069–2087.
- Douville, H. (2002), Influence of soil moisture on the Asian and African monsoons. Part II: Inter-annual variability, *J. Clim.*, *15*, 701–719.
- Douville, H., and F. Chauvin (2000), Relevance of soil moisture for seasonal climate predictions: A preliminary study, *Clim. Dyn.*, *16*, 719–736.
- Douville, H., F. Chauvin, and H. Broqua (2001), Influence of soil moisture on the Asian and African monsoons. Part I: Mean monsoon and daily precipitation, *J. Clim.*, *14*, 2381–2403.
- Drury, L. M. (1989), Advances in the study of sub-Saharan drought, *Int. J. Climatol.*, *9*, 77–90.
- Ebisuzaki, W. (1997), A method to estimate the statistical significance of a correlation when the data are serially correlated, *J. Clim.*, *10*, 2147–2153.
- Epstein, E. S. (1969), A scoring system for probability forecasts of ranked categories, *J. Appl. Meteorol.*, *8*, 985–987.
- Folland, C. K., T. N. Palmer, and D. E. Parker (1986), Sahel rainfall and worldwide sea temperatures, *Nature*, *320*, 602–607.
- Folland, C. K., J. Owen, M. N. Ward, and A. Colman (1991), Prediction of seasonal rainfall in the Sahel using empirical and dynamical methods, *Weather Forecast.*, *10*, 21–56.
- Fontaine, B., and S. Bigot (1993), West African rainfall deficits and sea surface temperatures, *Int. J. Climatol.*, *13*, 271–285.
- Fontaine, B., and S. Janicot (1996), Sea surface temperature fields associated with West African rainfall anomaly types, *J. Clim.*, *9*, 2935–2940.
- Fontaine, B., S. Janicot, and V. Moron (1995), Rainfall anomaly patterns and wind field signals over West Africa in August (1958–1989), *J. Clim.*, *8*, 1503–1510.
- Gadgil, S., and S. Sajani (1998), Monsoon precipitation in AMIP runs, *Clim. Dyn.*, *14*, 659–689.
- Garric, G., H. Douville, and M. Déqué (2002), Prospects for improved seasonal predictions of monsoon precipitation over West-Africa, *Int. J. Climatol.*, *22*, 331–345.
- Gates, W. (1992), The Atmospheric Model Intercomparison Project, *Bull. Am. Meteorol. Soc.*, *73*, 1962–1970.
- Giannini, A., R. Saranavan, and P. Chang (2003), Oceanic forcing of Sahel rainfall on inter-annual to interdecadal time scales, *Science*, *302*, 1027–1030.
- Goddard, L., S. J. Mason, S. E. Zebiak, C. F. Ropelewski, R. Basher, and M. A. Cane (2001), Current approaches to seasonal to inter-annual climate predictions, *Int. J. Climatol.*, *21*, 1111–1152.
- Goswami, B. N., V. Krishnamurti, and H. Annamalai (1999), A broad scale circulation index for the inter-annual variability of the Indian summer monsoon, *Q. J. R. Meteorol. Soc.*, *125*, 611–623.
- Gualdi, S., A. Navarra, and G. Tinarelli (1999), The inter-annual variability of the Madden-Julian Oscillation in an ensemble of GCM simulations, *Clim. Dyn.*, *15*, 643–658.
- Hansen, J., et al. (2002), Climate forcings in Goddard Institute for Space Studies S12000 simulations, *J. Geophys. Res.*, *107*(D18), 4347, doi:10.1029/2001JD001143.
- Hastenrath, S. (1990), Decadal scale changes of the circulation in the tropical Atlantic sector associated with Sahel drought, *Int. J. Climatol.*, *20*, 459–472.
- Janicot, S., V. Moron, and B. Fontaine (1996), Sahel droughts and ENSO dynamics, *Geophys. Res. Lett.*, *23*, 515–518.
- Janicot, S., A. Harzallah, B. Fontaine, and V. Moron (1998), West-African monsoon dynamics and eastern equatorial Atlantic and Pacific SST anomalies (1970–1988), *J. Clim.*, *11*, 1874–1882.
- Janicot, S., S. Trzaska, and I. Poccard (2001), Summer Sahel-ENSO teleconnection and decadal time scale SST variations, *Clim. Dyn.*, *18*, 303–320.
- Jetsu, L., and J. Pelt (1996), Searching for periodicity in weighted time point series, *Astron. Astrophys. Suppl. Ser.*, *118*, 587–594.
- Kalnay, E., et al. (1996), The NCEP-NCAR 40 year Reanalysis Project, *Bull. Am. Meteorol. Soc.*, *77*, 437–471.
- Kumar, A., and M. P. Hoerling (1995), Prospects and limitations of seasonal atmospheric GCM predictions, *Bull. Am. Meteorol. Soc.*, *76*, 335–345.
- Moron, V., B. Fontaine, and P. Roucou (1995), Global equatorial variability of 850 and 200 hPa zonal winds from rawinsondes between 1963 and 1989, *Geophys. Res. Lett.*, *22*, 1701–1704.
- Moron, V., A. Navarra, M. N. Ward, and E. Roeckner (1998), Skill and reproducibility of seasonal rainfall patterns in the tropics in ECHAM-4 GCM simulations with prescribed SST, *Clim. Dyn.*, *14*, 183–200.
- Moron, V., A. Navarra, M. N. Ward, C. K. Folland, P. Friederichs, J. Polcher, and K. Maynard (2001), Analysing and combining atmospheric general circulation model simulations forced by prescribed SST. Part I: Tropical response, *Ann. Geophys.*, *44*, 756–780.
- Moron, V., N. Philippon, and B. Fontaine (2003), Skill of Sahel rainfall variability in four atmospheric GCMs forced by prescribed SST, *Geophys. Res. Lett.*, *30*(23), 2221, doi:10.1029/2003GL018006.
- Oort, A. E. (1978), Adequacy of the rawinsonde network for the global circulation studies tested through numerical model output, *Mon. Weather Rev.*, *106*, 174–195.
- Oort, A. E., and H. Liu (1993), Upper-air temperature trends over the globe: 1958–1989, *J. Clim.*, *6*, 292–307.
- Palmer, T. N. (1993), Extended-range atmospheric prediction and the Lorenz model, *Bull. Am. Meteorol. Soc.*, *74*, 49–65.
- Palmer, T. N., and D. L. T. Anderson (1994), The prospect for seasonal forecasting: A review paper, *Q. J. R. Meteorol. Soc.*, *120*, 755–794.
- Palmer, T. N., C. Brankovic, P. Viterbo, and M. J. Miller (1992), Modeling inter-annual variations of summer monsoons, *J. Clim.*, *5*, 399–417.
- Palmer, T. N., et al. (2004), Development of a European Multi-model Ensemble System for Seasonal to Inter-annual Prediction (DEMETER), *Bull. Am. Meteorol. Soc.*, *85*, 853–872.
- Poccard, I., S. Janicot, and P. Camberlin (2000), Comparison of rainfall structures between NCEP/NCAR reanalyses and observed data over tropical Africa, *Clim. Dyn.*, *16*, 897–915.
- Rayner, N. A., E. B. Horton, D. E. Parker, C. K. Folland, and R. B. Hackett (1996), Version 2.2 of the global sea-ice and sea surface temperature data set, 1903–1994, *Clim. Res. Tech. Note 74*, 21 pp., Hadley Cent., Bracknell, UK.
- Rowell, D. P. (1998), Assessing potential seasonal predictability with an ensemble of multidecadal GCM simulations, *J. Clim.*, *11*, 109–120.
- Rowell, D. P. (2001), Teleconnections between the tropical Pacific and the Sahel, *Q. J. R. Meteorol. Soc.*, *127*, 1683–1706.

- Rowell, D. P., C. K. Folland, K. Maskell, and M. N. Ward (1995), Variability of summer rainfall over tropical North Africa (1906–1992), Observations and modeling, *Q. J. R. Meteorol. Soc.*, *113*, 669–674.
- Sperber, K. R., and T. N. Palmer (1996), Inter-annual tropical rainfall variability in general circulation model simulations associated with the Atmospheric Model Intercomparison Project, *J. Clim.*, *9*, 2727–2750.
- Srinivasan, G., M. Hulme, and C. G. Jones (1995), An evaluation of the spatial and inter-annual variability of tropical precipitation as simulated by GCMs, *Geophys. Res. Lett.*, *22*, 1697–1700.
- Stern, W., and K. Miyakoda (1995), The feasibility of seasonal forecasts speculated from multiple GCM simulations, *J. Clim.*, *8*, 1071–1085.
- Sud, Y. C., and K. M. Lau (1996), Comments on “Variability of summer rainfall over tropical North Africa (1906–1992), Observations and modelling” by Rowell et al. (1995), *Q. J. R. Meteorol. Soc.*, *22*, 1001–1006.
- Trzaska, S., V. Moron, and B. Fontaine (1996), Global atmospheric response to specific linear combination of the main SST modes. Part I: Numerical experiments and preliminary results, *Ann. Geophys.*, *14*, 1066–1077.
- Uppala, S. (2002), ECMWF reanalysis, 1957–2001, *ERA-40 Proj. Rep. Ser. 3*, Eur. Cent. for Medium-Range Weather Forecasts, Reading, UK.
- Ward, M. N. (1992), Provisionally corrected surface wind data, worldwide ocean-atmosphere surface fields and Sahelian rainfall variability, *J. Clim.*, *5*, 454–475.
- Ward, M. N. (1998), Diagnosis and short-lead time prediction of summer rainfall in tropical North Africa at inter-annual and multidecadal time-scales, *J. Clim.*, *11*, 3167–3191.
- Webster, P. J., and S. Yang (1992), Monsoon and ENSO: Selectively interactive systems, *Q. J. R. Meteorol. Soc.*, *118*, 877–926.
- Wolter, K., and M. Timlin (1998), Measuring the strength of ENSO events: How does 1997/98 rank?, *Weather*, *53*, 315–324.
-
- B. Fontaine and N. Philippon, CRC, UMR 5080-CNRS, Université de Bourgogne, 6, Bd Gabriel, F-21004 Dijon Cedex, France.
- V. Moron, International Research Institute for Climate Prediction, Palisades, NY 10964-8000, USA. (vincent@iri.columbia.edu)